



Gold Nano-Structures for Transduction of Biomolecular Interactions into Micrometer Scale Movements

Nickolay V. Lavrik,^{1*} Christopher A. Tipple,¹
Michael J. Sepaniak,^{1*} and Panos G. Datskos²

¹Department of Chemistry, University of Tennessee, Knoxville,
Knoxville, TN 37919

²Engineering Technology Division,
Oak Ridge National Laboratory, Oak Ridge, TN 37831

Abstract. Microfabricated cantilevers, similar to those commonly used in scanning probe microscopies, have recently become increasingly popular as transducers in chemical and biological sensors. Surface stress changes that accompany intermolecular interactions on the cantilever surfaces offer an attractive means to develop new generations of microfabricated sensors and actuators that respond directly to chemical stimuli. In the present study, we demonstrate that interfacial molecular recognition events can be converted into mechanical responses much more efficiently when quasi 3-dimensional interfaces with nano-size features are used. Some of the particularly useful approaches to creating such interfaces are surface immobilization of gold nano-spheres and dealloying of co-evaporated Au:Ag films. Preliminary evaluation of these nanostructured surfaces was performed by measuring mechanical stresses generated by receptor modified nano-structures and smooth gold surfaces in response to gas-phase hydrocarbon compounds. The most efficient chemi-mechanical transduction was achieved when the cantilevers were modified with 50 to 75 nm thick dealloyed gold nanostructures. Cantilevers of this type were selected for liquid phase experiments. These cantilevers were found to undergo several micron deflections upon adsorption of protein A and biotin-labeled albumin on nanostructured gold surfaces. Additional micrometer scale movements of the cantilevers were observed upon interaction of the surface bound bioreceptors with, respectively, immunoglobulin G and avidin from the aqueous phase.

Key Words. actuator, BioMEMS, cantilever, colloidal gold, immunosensor, nanoparticles

Introduction

One of the essential differences between microelectromechanical systems (MEMSs) and conventional (macroscopic) mechanical systems is a dramatically increased surface-to-volume ratio. As a result, surface forces that can be ignored on macroscales can play an important or even a key role in the functioning of MEMS devices. Although surface forces rarely extend from surfaces beyond the nanoscale (Israelachvili, 1991), their integral effects can influence macroscopic behavior of many systems with large surface-to-volume ratios. Normal and lateral components of surface forces are

usually displayed on the macroscale through adhesion and deformation, respectively. Examples demonstrating such cumulative macroscopic effects of surface forces span from the formation of droplets and floating monolayers to the integrity of a biological tissue. As applied to BioMEMS, surface forces often result in undesirable effects, such as protein fouling and increased backpressure in microchannels. Conversely, a significant contribution of surface forces into the total energy accumulated in MEMS can be used as a principle of chemi-mechanical transduction.

By measuring deformations of a thin plate, surface stress changes associated with unequal adsorption of chemical species on the sides of this plate can be monitored. This method, commonly referred to as a beam-bending technique (Frink and van Swol, 2000), had limited applications until macroscopic plates were replaced with much smaller microfabricated cantilevers (typically 0.2–1 μm thick, 20–100 μm wide and 100–500 μm long) similar to those used in scanning probe microscopy. Microcantilevers (MCs) permit measurements of surface stress changes in the low mN m^{-1} range and are becoming increasingly popular as transducers in chemical and biological sensing (Thundat et al., 1995; Harris et al., 1996; Thundat, et al. 1997; Varesi et al., 1997; Datskos and Sauers, 1999; Raiteri et al., 1999; Baller et al., 2000; Betts et al., 2000; Fagan et al., 2000; Fritz et al., 2000; Ji et al., 2000; Moulin et al., 2000). The growing fundamental and practical interest in cantilever-based sensors can be explained by the following two factors. Firstly, the sensitivity of MCs to minute quantities of adsorbates is superior to that of many other transducers. For instance, the MCs offer much better mass sensitivity as compared to gravimetric resonating devices. Secondly, a MC transducer directly converts changes in the Gibbs free

*Corresponding authors.

This paper is based on a presentation made at BioMEMS and Biomedical Nanotechnology World 2000.

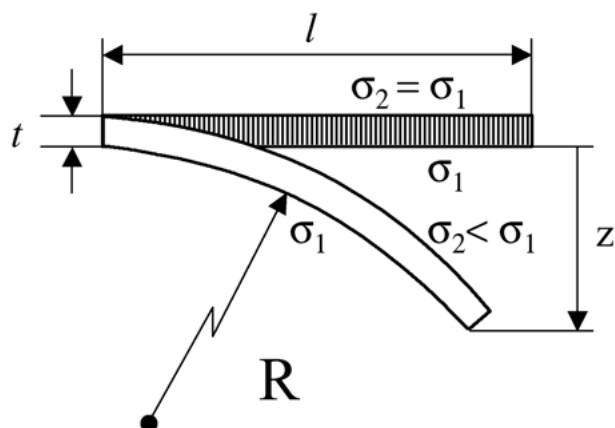


Fig. 1. Circular bending of a cantilever induced by a differential stress due to unequal changes of interfacial energies on each of the cantilever sides.

energy due to analyte-surface intermolecular interactions into measurable mechanical response. This means that MC transducers are equally functional in both gases and liquids and can be functionalized with variety of synthetic or biological receptors.

Using micromachined cantilevers, surface stress changes associated with non-specific (Butt et al., 1996; Moulin et al., 1999; Moulin et al., 2000) and specific (Raiteri et al., 1999; Fritz et al., 2000) protein-surface interactions have been recently monitored. However, the measured nanoscale cantilever deflections in response to the protein binding events appear to be barely above the detectable level. While cantilever deflections smaller than 10^{-10} m can be reliably detected in the gas-phase, a much poorer limit of detection has been achieved in liquids because of instabilities associated with temperature, flow (Butt, 1996) and ion exchange effects (Lang and Heusler, 1995). Improvement in ability to perform cantilever deflection measurements in liquids can be achieved using a differential scheme that effectively reduces certain sources of noise (Fritz et al., 2000). Alternatively, it is important to identify fundamental mechanisms that would lead to more efficient transduction of interfacial interactions into mechanical responses and hence larger output signals. It should be noted that intermolecular and intersurface forces have been extensively studied, both experimentally and theoretically, in their relation to behavior of colloidal systems (Israelachvili, 1991) and biomimetic membranes (Leckband et al., 1994; Leckband, 1995; Leckband et al., 1995; Sivasankar et al., 1999; Lavrik et al., 2000). This knowledge also can be used in the design of highly responsive cantilever-based chemi-mechanical transducers. The present study shows that a dramatically increased efficiency of chemi-mechanical transduction results from asymmetric nanostructuring of MCs.

Mechanisms of Chemi-Mechanical Transduction

Cantilevers with smooth surfaces

When surface stresses σ_1 and σ_2 on each side of the cantilever change unequally, the equilibrium state of the cantilever is disturbed causing bending (Figure 1). The resulting deformation can be characterized by the radius of cantilever curvature, R , or tip deflection $z = l^2/2R$. The effect of surface stress change on cantilever bending is quantified by Stoney's equation (Stoney, 1909; von Preissig, 1989):

$$\frac{1}{R} = \frac{6(1-\nu)}{Et^2} \Delta\sigma \quad \text{and} \quad z_{\max} = \frac{3l^2(1-\nu)}{Et^2} \Delta\sigma \quad (1)$$

where ν and E are, respectively, the Poisson's ratio and Young's modulus for the cantilever, t is thickness of the MC, l is cantilever effective length and $\Delta\sigma = \sigma_2 - \sigma_1$ is a differential surface stress. Although Stoney's equation (1) does not account for a multi-layer structure of cantilevers that are typically used in sensor applications, it gives a fair approximation as long as the over-layers are thin in comparison to the substrate material.

If one side of the MC is relatively passive (i.e., non-adsorbing), the changes in $\Delta\sigma$ are caused primarily by the modulation of interfacial energy of the other side, $\Delta\gamma_2$.

$$\Delta\sigma = \gamma_{2,f} - \gamma_{2,i} = \Delta\gamma_2 = \Delta G_2 \Gamma M^{-1}. \quad (2)$$

In equation (2) $\gamma_{2,f}$ and $\gamma_{2,i}$ are final and initial (post and pre adsorption) interfacial energies, ΔG_2 is a change in Gibbs free energy caused by the adsorption process, Γ is the mass of adsorbate per unit area and M is the molar mass of the adsorbate material. Equation (2) shows that any spontaneous adsorption process ($\Delta\gamma_2$ negative) is driven by an excess of surface free energy and can only reduce the surface free energy of the substrate. Therefore, a surface stress change caused by spontaneous adsorption is always compressive. Importantly, the larger the initial surface free energy of the substrate, the greater the possible change in surface stress resulting from spontaneous adsorption processes. Among all materials, pure metals have the highest surface free energies and are especially useful as modifying coatings for MC-based chemi-mechanical transducers. For instance, the surface free energy of pure gold in air is approximately 1.2 N m^{-1} (de Boer et al., 1988) while the interfacial energy of a typical gold-hydrocarbon interface calculated according to Lifshitz theory is about 0.9 N m^{-1} (Israelachvili, 1991). By this treatment the expected value of $\Delta\gamma_2 = 0.3 \text{ N m}^{-1}$ (surface stress of hydrocarbon adsorbates in contact with an outer gas medium

does not exceed 0.03 N m^{-1} (Israelachvili, 1991) and is neglected). This estimate is consistent with the maximal changes in surface stresses observed on gold surfaces in response to the vapor phase chemisorption of alkanethiols (Berger et al., 1997). In order to predict maximal responses of cantilever based chemi-mechanical transducers in water, an interfacial energy of the substrate-water interface rather than surface free energy of the substrate material should be taken into account. Because of very strong interactions between two materials with high surface free energies, interfacial energies of metal-water interfaces are strongly reduced in comparison to the surface free energies of the same metals in the gas phase. Even lower interfacial energies ($<0.05 \text{ N m}^{-1}$) characterize interfaces between water and materials other than metals. This imposes a strong limitation on maximal surface stress changes that may result from binding events at organic-modified interfaces in an aqueous phase.

For substrate and adsorbate phases in contact the interfacial energy can also be evaluated using the Dupré equation

$$\gamma_2 = \gamma_{\text{sub}} + \gamma_{\text{ads}} - W_{\text{adh}} \quad (3)$$

where γ_{sub} and γ_{ad} are surface free energies of the substrate and the adsorbate, respectively, and W_{adh} is the work of adhesion between the substrate and the adsorbate. Note that W_{adh} accounts for the surface density of adsorbate molecules. In the case of gas-phase physisorption and occupancies up to a closely packed monomolecular layer, W_{adh} is nearly proportional to the binding energy per adsorbate molecule and the density of the receptor on the surface as seen in equation (4)

$$W_{\text{adh}} = E_{\text{ads}} \Gamma M^{-1} \quad (4)$$

where E_{ads} is binding energy per mole of the adsorbate. Combining equations (2)–(4) and assuming $\gamma_{\text{ads}} \ll W_{\text{adh}}$, we obtain the expression for $\Delta\sigma^{\text{max}}$, an upper limit of adsorbate-induced surface stress

$$\Delta\sigma^{\text{max}} = E_{\text{ads}} \Gamma M^{-1}. \quad (5)$$

It should be noted that equation (4) does not account for interactions with an aqueous medium explicitly and that the Dupré equation may not be valid in the case of specific biomolecular interactions. Nevertheless, this equation does predict an upper limit for surface stress changes that result from reversible interfacial processes, including those that involve specific binding of biological analytes to receptor-modified surfaces. This prediction is based on the energy conservation principle. In the case of biomolecular interactions E_{ads} , Γ , and M in

equation (5) become the receptor-analyte binding energy, the analyte surface density, and the analyte molar mass, respectively. According to this analysis, a monolayer of protein with a medium affinity ($E_{\text{ads}} = 10 \text{ Kcal mol}^{-1}$), medium molecular weight (100 KDa), and a surface density of 2 mg m^{-2} will cause *ca.* 1 mN m^{-1} change in surface stress. This corresponds to 2 to 5 nm deflections of a typical MC. Binding of smaller, higher-affinity or more densely packed biological molecules will produce respectively larger mechanical responses. These predictions are consistent with the recently reported 10 to 20 nm deflections of MCs observed in response to oligonucleotide hybridization and protein A-immunoglobulin G (IgG) interactions (Fritz et al., 2000). However, a change in surface stress caused by adsorbate molecules that occupy a very small fraction of a smooth surface is likely to be below the noise level.

When analyte species interact with the bulk of a thick modifying coating, swelling of the latter, rather than reduction of the interfacial energy, becomes a predominant mechanism of cantilever deflection. In this case, integral analyte-induced stress within the coating scales up in proportion to the coating thickness. Fifty nanometers to $10 \mu\text{m}$ thick coatings have been shown to produce substantial compressive stresses in response to gas-phase analytes (Thundat et al., 1995; Maute et al., 1999; Baller et al., 2000; Betts et al., 2000; Fagan et al., 2000). However, synthesis of materials that are bulk-accessible for macromolecular analytes is complicated. In addition, deformations of thicker gel-like receptor layers would adversely affect propagation of mechanical responses from receptor sites within the coating to the cantilever surface. Therefore, rational design of modifying coatings for chemi-mechanical transducers relies on a trade-off involving several factors. As demonstrated herein, the limitations of this trade-off can be surmounted using quasi 3-dimensional nanostructured interfaces.

Expected effects of nanostructured surfaces

Theoretical evaluations as well as direct measurements of solvation forces (Israelachvili, 1991) provide strong evidence that integral stresses (calculated per geometrical area of the sample) within surface-confined colloids or nanoporous films (Frink and van Swol, 1999; Frink and van Swol, 2000) may exceed the “true” surface stress of smooth solids by several orders of magnitude. Although rigorous theoretical evaluation of adsorbate-induced stresses at the nanostructured interfaces is beyond the scope of the present study, some important conclusions can be made using the following simplified model. When receptor molecules are very densely packed on the MC surface, or in the case of thicker (multilayer) modifying coatings and/or surfaces with 3-dimensional nanosize features (such as shown in

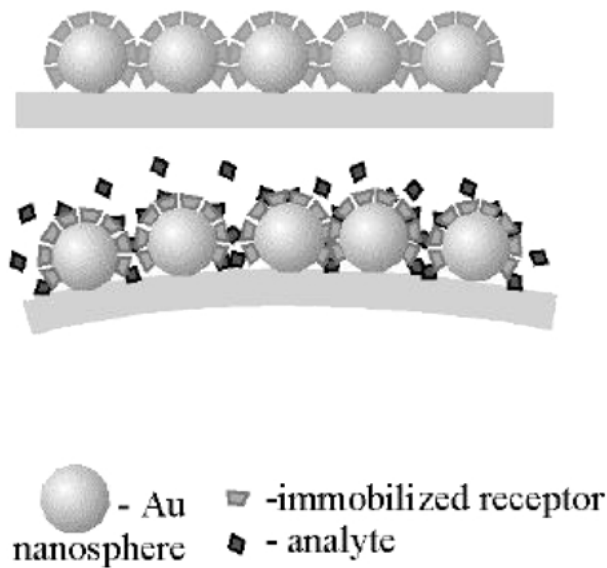


Fig. 2. Schematic illustration of surface immobilized colloid. In the case of gold colloidal particles, the resulting nanostructured surface can be modified with appropriate receptors using gold-thiol reaction schemes. Intersurface forces within such a nanostructured layer calculated per projected surface may substantially exceed interfacial energy for any smooth interface.

Figure 2), analyte binding can induce surface stress changes through additional mechanisms. Subnanometer intermolecular gaps are normally associated with strong steric repulsion (Israelachvili, 1991). An in-plane component of the steric repulsion is difficult to express analytically, however, it will act to reduce interfacial energy similarly to the adhesive term, W_{ads} in equation (3). Thus, equation (3) can be modified as follows

$$\gamma_2 = \gamma_{\text{sub}} + \gamma_{\text{ads}} - W_{\text{adh}} - W_{\text{ster}} \quad (6)$$

where W_{ster} represents an additional term that accounts for in-plane steric repulsive forces due to adsorbate confinement on a surface or within a nanostructured coating. In the case of thicker receptor-immobilizing coatings, solvation of analyte molecules in the bulk of a receptor phase involves additional steric, osmotic, hydration and electrostatic forces. The contribution from these additional forces into effective surface stress scales up in proportion with the thickness of the receptor phase and, in principle, is not limited by the initial interfacial energy of the substrate-medium interface. However, stress-slip conditions will arise when surface stresses produced by a thicker coating on a smooth surface approach the energy of substrate-coating adhesion or substrate-coating molecular friction. As a rule, the latter values are below surface free energy of a substrate material. In addition to involvement of additional mechanisms that lead to enhanced adsorbate-

induced stresses, the expected role of nanostructured surfaces is to prevent stress-slip conditions independently of the substrate surface free energy. It should also be noted that theoretical calculations predict the possibility of both tensile and compressive adsorbate-induced stresses in nanoporous coatings.

Technological approaches to nanostructured surfaces

Several well-established technological strategies can be used to create nanostructured surfaces. These include electrochemical deposition, catalytic growth and high-pressure physical vapor deposition. However, application of such technologies to cantilevers is a challenging task. Two technological strategies that are more compatible with chemi-mechanical transducers have been identified in the course of the present work. The first strategy (Figure 3, Scheme I) utilizes pre-formed nano-sized building blocks, such as colloidal particles and molecular aggregates, which can be assembled on surfaces using covalent or electrostatic interactions. This method has been extensively explored to prepare assemblies of gold nanoparticles on glass, silicon and gold substrates (Grabar et al., 1996) and has been employed in our prior work (Lavrik et al., 2000) on vapor-phase cantilever-based sensors. The second strategy takes advantage of segregated nanophases that exist in many composite materials, for instance Au:Ag alloys. Selective removal of one phase from the bulk of these composite materials will release a nanostructured layer. This methodology has been previously used by Li and Sieradzki (1992) to prepare bulk samples of nanoporous gold that, depending on the annealing regime, exhibited pore distribution in the range of 10–1000 nm. However, the reported procedures included electrochemical dealloying of Au:Ag samples in nitric

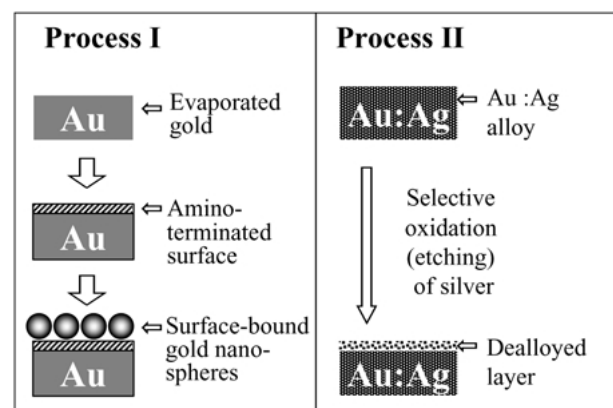


Fig. 3. Two approaches to creating gold nanostructures suitable for applications in cantilever-based chemi-mechanical transducers. Process I: Immobilization of gold colloid on smooth gold surface. Process II: Dealloying of Au:Ag composite films.

acid and were not readily applicable to MCs. In the present studies, we introduce rapid chemical de-alloying of Au:Ag co-evaporated films under much less harsh conditions thus creating nanostructured gold coatings (Figure 3, Scheme II) in a manner that is highly compatible with MCs as well as with MEMS in general.

Materials and Methods

Chemicals

Gold (99.99%), silver (99.999%) and chromium (99.99%) for vacuum evaporation were obtained from Gatewest Co., Alfa Aesar, and Kurt J. Lesker Company, respectively. Tetrachloroethylene (TCE), Hydrogen tetrachloroaurate (HAuCl_4), octadecylthiol (ODT), 4-aminothiophenol (4-ATP), mercaptoethane (EtSH) and colloidal gold with mean diameter of 20 nm were purchased from Sigma and used as received. The salts for preparation of phosphate buffer solutions (PBS), concentrated sulfuric acid and hydrogen peroxide used in these studies were purchased either from Sigma or Fisher Scientific. These reagents were of the highest available grade and used as received. All water used to prepare solutions was obtained from a Barnstead E-Pure water filtration system. Ultra high purity nitrogen was used as the carrier gas in gas-phase experiments. Heptakis-6-mercapto- β -cyclodextrin (HM- β -CD) was synthesized according to the method of Stoddart et al. (Rojas et al., 1995). Protein A (Extracellular protein A from *Staphylococcus aureus*), human immunoglobulin G (IgG, reagent grade), biotin-labeled albumin (biotin-albumin) and avidin were purchased from Sigma. Binding activity of the proteins and resulting surface coverage on smooth gold surfaces was verified using a computerized surface plasmon resonance (SPR) set-up described previously (Lavrik and Leckband, 2000).

Cantilever modification

In reference experiments, triangular, gold-coated silicon nitride cantilevers (Figure 4) purchased from Park Scientific Inc. were used directly after washing in a piranha bath (75% H_2SO_4 , 25% H_2O_2) for 2–3 minutes followed by thorough rinsing in deionized water. Pre-cleaned gold-coated cantilevers were also used for subsequent chemical or/and structural modifications. Alternatively, the original gold layer was removed from some cantilevers in a mixture of nitric and hydrochloric acids (3:1 volume ratio) and a new nanostructured metalization was created as described below.

In order to create gold nano-structures on one side of the cantilevers, two different technological strategies were used. According to the first strategy (Process I in Figure 3), the cantilevers with pre-cleaned evaporated

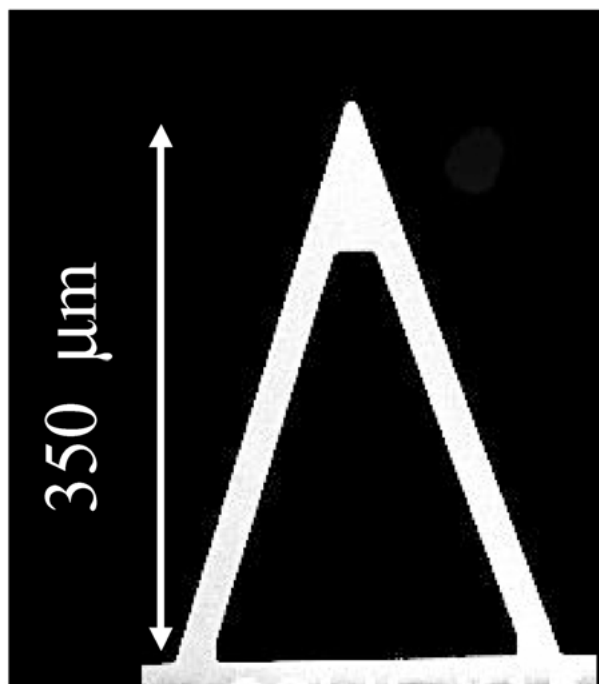


Fig. 4. Microphotograph of a silicon nitride cantilever used in these studies.

gold were treated in 1 gL^{-1} 4-ATP solution in methanol for 3–4 hours and rinsed successively in methanol and water. 4-ATP-modified cantilevers were placed in a 0.01% (w/v) gold colloid (20 nm gold nanospheres suspended in pure water). After modifying, the cantilever was then removed from the solution and gently washed with water.

According to the second strategy (Process II in Figure 3), a composite metal coating was created on one side of bare silicon nitride cantilevers using thermal evaporation in vacuum from tungsten boats. Evaporation of a 4 nm chromium adhesion layer was followed by evaporation of a 15 nm gold layer and, without stopping the evaporation of gold, by co-evaporation of gold and silver until a composite Au:Ag film of the desirable thickness was formed. Twenty to 100 nm thick co-evaporated Au:Ag layers were used in our studies. Both the deposition rates and resulting coating thickness were monitored using a quartz crystal microbalance. The deposition rates were 0.02 and 0.04 nm s^{-1} during evaporation of chromium and gold, respectively. During co-evaporation of gold and silver, the mass deposition rates were the same for the both metals unless otherwise noted. Silver was subsequently etched out of the composite films by placing the cantilever in an aqueous solution of 0.2 w/v % HAuCl_4 for 2–3 minutes. Cantilevers were rinsed with copious amounts of water after etching.

For preliminary gas-phase experiments cantilevers with smooth and nanostructured gold coatings were covalently modified with either mercaptoethane or HM- β -CD. Selective attachment of EtSH and HM- β -CD to the gold surfaces was carried out in 1 mM solutions of these agents for 18–20 hours as described elsewhere (Rojas et al., 1995). Upon removal from the solutions, the cantilevers were rinsed with copious amounts of the solvent and then water. Methanol and DMSO/water (3 : 2 volume ratio) were used as solvents for EtSH and HM- β -CD, respectively.

Cantilever deflection measurements

Cantilever deflection measurements were carried out according to optical lever detection scheme. Our set-up (Figure 5) included a 5 mW diode laser (Coherent Co., mW) operating at 632 nm, a spatial filtering and focusing system and a position sensitive optical detector. The output signal was displayed and recorded using a multichannel digital recorder (Stanford Research Systems). A 1 mL flow cell housing a cantilever holder was used for vapor-phase measurements. Gaseous analytes were delivered into the cell via a syringe pump through a T-joint and a 4-way valve, which enabled switching between pure nitrogen and diluted analyte. The degree of analyte dilution was defined by the syringe pump flow rate divided over a total flow rate. The latter was measured at the cell outlet using a mass

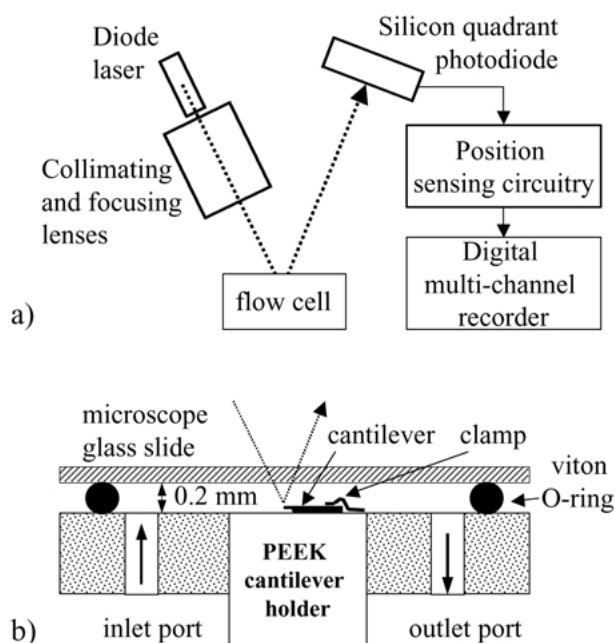


Fig. 5. Schematics of (a) the experimental set-up for optical detection of cantilever deflections and (b) the flow-cell for liquid-phase measurements.

flow meter tube. A flow rate of $3 \pm 0.3 \text{ mL min}^{-1}$ was used in the gas-phase experiments.

For liquid phase-measurements, a cantilever was mounted inside a smaller volume (approximately $100 \mu\text{L}$) teflon flow cell (Figure 5b) that provided a nearly laminar flow in the cantilever vicinity. A system of vessels connected to three-way valves allowed for switching between different solutions with minimal disturbance of the flow. Gravity driven flow was adjusted to a rate of $0.15 \pm 0.02 \text{ mL min}^{-1}$. The entire apparatus was placed on a vibration isolation table (Newport, RS2000) located in a thermally controlled environment.

Results and Discussion

Preliminary characterization of gold nanostructures

Our preliminary experiments were aimed to verify that electrostatic assembling of colloidal gold and dealloying of Au:Ag composites result in surfaces with desirable nanoscale features. Figure 6 shows the unprocessed AFM images of the nanostructured surfaces of the two types. These typical images clearly confirmed a high density of 20 nm gold spheres (Figure 6A) assembled on 4-ATP-modified gold surfaces and larger irregular gold clusters formed as result of dealloying Au:Ag films (Figure 6B). An apparent feature of the imaged samples is their

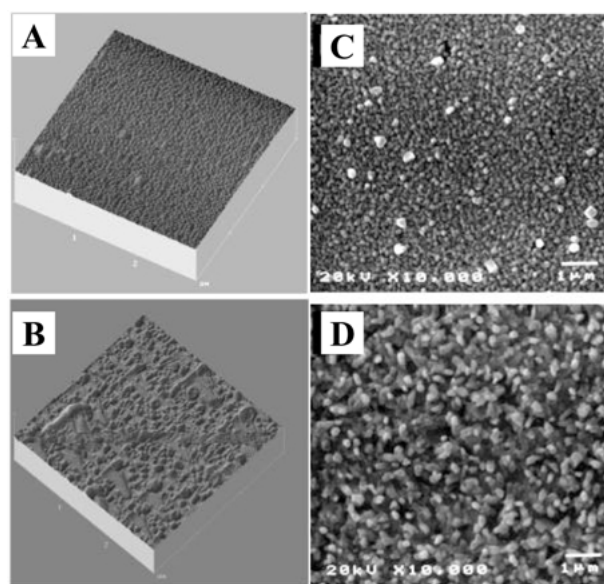


Fig. 6. AFM images of gold nanospheres assembly (panel A) and 20 nm thick dealloyed gold coating (panel B). Both scan areas are $3 \mu\text{m} \times 3 \mu\text{m}$. SEM images of 20 nm (panel C) and 75 nm (image D) dealloyed gold coatings.

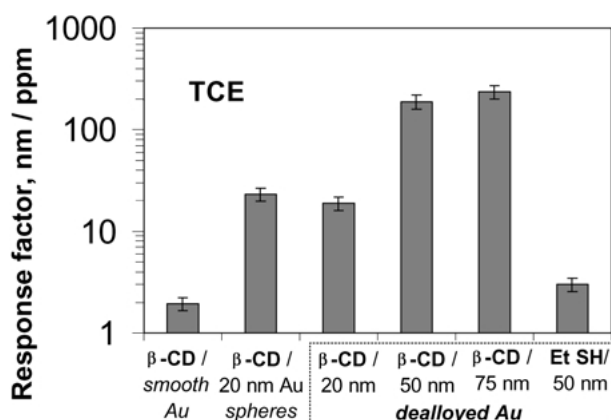


Fig. 7. Comparison of normalized deflection responses of HM-β-CD modified cantilevers with smooth and nanostructured gold surfaces to vapor phase TCE. The response factors were calculated using linear regression analysis of the calibration plots measured for 0.6 to 60 ppm TCE in dry nitrogen.

increased surface area and roughness as compared to conventionally evaporated gold (not shown). It should be noted, however, that a finite AFM tip curvature always introduces strong distortion (flattening) when imaging very deep crevices. Since such features were anticipated in the case of dealloyed gold coatings, SEM images (panels C and D in Figure 6) of these samples were obtained to complement the topographic information provided by AFM. Indeed, the SEM images confirmed presence of the narrow gaps between gold clusters of the size favorable for involvement of short-range van der Waals, solvation, and steric forces. These quasi 3-dimensional nano-structures may be interpreted as surface confined colloids rather than porous solids. Comparison of dealloyed gold coatings of different thicknesses (panels C and D in Figure 6) also indicates a dependency of the gold cluster sizes on the initial thickness of the co-evaporated coating.

Preliminary comparative characterization of cantilevers with smooth gold and gold nanostructures was performed in the gas phase. TCE and HM-β-CD were used as a convenient receptor-analyte pair of practical and fundamental importance. Linear regression analysis was applied to calibration plots obtained for TCE with differently modified cantilevers. Figure 7 depicts a summary of this analysis. Detailed results on the deflections of nanostructured cantilevers observed in response to various vapor phase analytes are reported elsewhere (Lavrik and Leckband, 2000). As can be seen in Figure 7, nanostructuring of the gold surfaces lead to dramatic increases in response factors (deflection response normalized by analyte concentration) for HM-β-CD-modified cantilevers. Enhancement factors (response factor for nanostructured cantilever/response factor for smooth gold cantilever) exceeded two orders of

magnitude in the case of the thicker (50 to 75 nm) dealloyed gold coatings. It is also important to note that 50 nm thick nanostructured gold coatings derivatized with a short-chain (ethyl) mercaptane also provide enhanced responses to TCE. However, as compared to cantilevers with HM-β-CD-modified cantilevers, the response factor is considerably less. This observation correlate well with the fact that HM-β-CD exhibits receptor properties with regard to TCE molecules. Therefore, preserved receptor properties of the molecules on the prepared nanostructures are anticipated. Because the most encouraging results were obtained with dealloyed gold coatings, cantilevers with this type of nanostructures were selected for our subsequent aqueous phase experiments.

Stresses induced by protein-surface and protein-protein interactions on different surfaces

In liquid-phase experiments, MCs mounted in the flow cell were first pre-equilibrated in deionized water for 15 minutes and then in a 10 mM phosphate buffer saline (PBS) solution at pH = 7.2 for 1 to 2 hours. This minimized drifts in output signal observed without the pre-equilibration procedure.

In the first series of experiments, the MCs were *in-situ* functionalized with biotin by flowing 0.05 g L⁻¹ solution of biotin-labeled albumin (biotin-albumin) in PBS (pH = 7.2) for approximately 25 minutes. Adsorption of biotin-albumin on bare gold under these conditions was verified independently using SPR and found to yield protein surface density of 0.8 ± 0.1 mg m⁻². It should be emphasized that more than 90% of the equilibrium protein coverage was formed in the first five minutes of the adsorption.

The magnitude and the directions of the MC deflections during adsorption of biotin-labeled albumin depended strongly on the type of cantilever surface. As expected, cantilevers with hydrophobized (ODT-modified) smooth gold exhibited practically no measurable deflection (Figure 8, curve 1). However, when an identical cantilever with smooth gold was pre-cleaned in a piranha solution (mixture of H₂SO₄ and H₂O₂ with a 3 : 1 volume ratio) for 2–3 minutes at 35°C, adsorption of biotin-albumin caused substantial cantilever deflection that corresponds to a compressive surface stress change $\Delta\sigma = -0.2 \text{ N m}^{-1}$ (Figure 8, curve 2). This value is close to the estimated difference between interfacial energies for gold-water and gold-hydrocarbon interfaces and, therefore, can be explained within the models of adsorption-induced stresses discussed above. Adsorption of biotin-albumin on MCs with 50 nm dealloyed gold coatings resulted in a *ca.* 4 micron deflection (Figure 8, curve 3) and, respectively, in an extremely large tensile surface stress change, $\Delta\sigma = 1.25 \text{ N m}^{-1}$. The kinetics

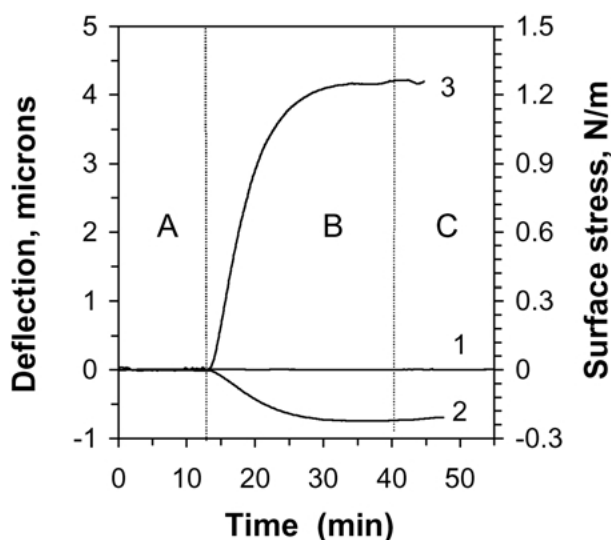


Fig. 8. Cantilever deflections and changes in effective surface stress induced by immobilization of albumin-biotin conjugate on different surfaces. One side of the silicon nitride cantilever was coated with: 40 nm smooth gold that precleaned in piranha bath and additionally hydrophobized with octadecylthiol before the experiment (1); 40 nm smooth gold that was piranha-cleaned just before the experiment (2), 50 nm dealloyed gold containing 50% Au (3). Regions A–C of the graph correspond to the following cell content: A—buffer (10 mM PBS, pH = 7.2 + 10 mM NaNO₃); B—0.05 g L⁻¹ biotin-albumin in the same buffer; C—buffer. A constant flow rate of 0.15 mL per minutes was maintained during the experiments.

of cantilever deflections was rather slow in the case of both smooth and nanostructured gold coatings. As discussed previously (Moulin, 1999) this indicates that slow post-binding protein rearrangement contributes to MC deflections.

The cantilevers with 50 nm dealloyed gold, proven to be highly efficient in responding to nonspecific adsorption of biotin-albumin, were additionally used to monitor specific biotin-avidin interaction. Figure 9 shows responses of the cantilever with 50 nm dealloyed gold coating caused by sequentially changed composition of the flow cell. avidin-biotin interaction. The cantilever deflection reached *ca.* 2 μm in 50 minutes after 0.025 g L⁻¹ avidin was added into the buffer flowing through the cell. Upon flushing the cell with pure buffer, the response somewhat reversed. Since dissociation of unloaded biotin-avidin bonds is extremely slow (Evans and Ritchie, 1997) the observed rather rapid shift of the binding equilibrium in absence of avidin indicates that an extremely large surface stress generated upon biotin-avidin interaction may, in turn, facilitate biotin-avidin dissociation. In other words, an apparent binding constant decreases when a substantial part of the total energy of receptor-ligand interactions in the system is converted into mechanical energy (Parsegian and Podgornik, 1997).

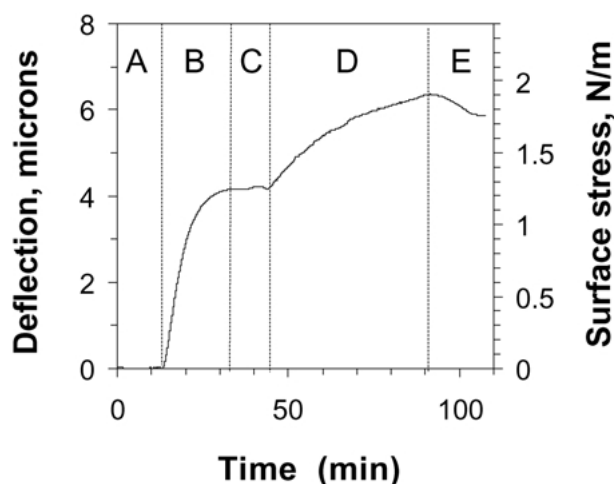


Fig. 9. Deflections of the cantilever with 50 nm dealloyed gold and corresponding changes in effective surface stress induced by immobilization of biotin-avidin conjugate and subsequent interactions between thus immobilized biotin and avidin from solution. Regions A–C of the graph correspond to the following cell content: A—buffer (10 mM PBS, pH = 7.2 + 10 mM NaNO₃); B—0.05 g L⁻¹ biotin-albumin in the same buffer; C—buffer; D—0.025 g L⁻¹ avidin in the buffer; E—buffer.

In the next series of experiments the cantilevers were *in-situ* functionalized with protein A that has high affinity (Moks et al., 1986) to a F_(c) fragment of IgG from many mammals. This was achieved by flowing 0.05 g L⁻¹ protein A solution in PBS for 10 to 15 minutes. Binding of protein A to cantilevers with smooth gold was typically accompanied by deflections barely detectable from noise level (Figure 10, curve 1). As recently reported (Fritz et al., 2000) differential measurements carried out using cantilever arrays were necessary to distinguish thermal noise/drifts and subtle changes in surface stress associated with interactions between protein A immobilized on a smooth cantilever surface and IgG in solution. Although Protein A is known to form well-packed monolayers on gold (Guilbault et al., 1992) its nonspecific adsorption on the silicon nitride side of the MCs may have occurred as well. This is one of the factors that could reduce the differential surface stress changes observed upon immobilization of the protein on cantilevers with smooth surfaces.

Similarly to biotin-avidin assays, both immobilization of protein A and subsequent protein A-IgG interaction could readily be monitored using asymmetrically nanostructured MCs. As can be seen in Figure 10, the cantilever with 20 nm thick dealloyed gold coating underwent approximately 0.1 μm and 0.4 μm deflections upon immobilization of protein A and subsequent Protein A-IgG interactions, respectively (Figure 10, curve 2). The use of thicker, 50 nm and 75 nm, nanostructured gold coatings lead to further enhancement of the generated

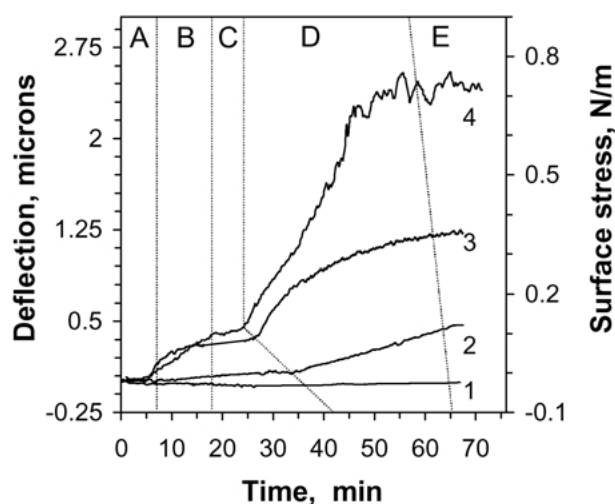


Fig. 10. Cantilever deflections and changes in effective surface stress induced by immobilization of Protein A and subsequent protein A–IgG assays on different surfaces. One side of the cantilevers was coated with: 35 nm smooth gold (1), 20 nm dealloyed gold (2), 50 nm dealloyed gold (3), and 75 nm dealloyed gold (4). Regions A–E of the graph correspond to the following cell content: A—buffer (10 mM PBS, pH = 7.2 + 10 mM NaNO₃); B—0.05 g L⁻¹ protein A in the same buffer; C—buffer; D—0.05 g L⁻¹ human IgG in the buffer; E—buffer. Note: regions A–C reflect in-situ immobilization of the protein A onto a cantilever surface; regions D and E show the effect of IgG on the cantilevers with immobilized protein A.

surface stresses and MC deflections (Figure 10, curves 3 and 4). The behavior of the asymmetrically nanostructured MCs is in a stark contrast to that of the cantilevers with smooth surfaces. In comparison to smooth gold, 50 nm dealloyed gold coating increases MC deflections by at least two orders of magnitude while only slightly larger noise was observed (Figure 10, curve 3). However, a substantially increased noise observed in the case of protein A–IgG interactions on 75 nm thick dealloyed gold (Figure 11, curve 4) may indicate mechanical instabilities that take place when induced stresses approach mechanical strength of the dealloyed gold coating.

The tensile surface stress changes induced by protein-surface and protein-protein interactions on the created nanostructured surfaces are not unusual (Moulin, 1999). They indicate an abundance of short-range attractive interactions between protein molecules at the created nano-structured interfaces. Similar attractive forces cause aggregation of proteins on various solid surfaces and were also observed at nanometer separations between interdigitated monolayers of polymers and proteins (Israelachvili et al, 1991; Sivasankar et al., 1999). Large observed enhancements in generated stresses can be explained by a dramatically increased number of close protein-protein interactions on the nanostructured side of the MC. Tensile adsorption-induced surface stress changes may also arise due to

altered electrostatic interactions, in particular, when protein binding reduces effective density of surface charges localized at the cantilever-water interface. This may occur through several mechanisms, such as compensation of charges on the MC surface by oppositely charged groups on the protein surface or hindering water accessibility.

Conclusions

We have shown that the asymmetric nanostructuring of MC surfaces can lead to two orders of magnitude enhancements in chemi-mechanical transduction. The magnitude of the effective surface stresses generated at the quasi 3-dimensional interfaces significantly exceeds surface free energies of common solids as well as adhesion energies of coating-substrate pairs frequently used in chemical sensors. Because the implemented asymmetric nanostructuring only slightly increases the deflection noise of the MC in equilibrium, it provides an approach to chemical sensors and biosensors with significantly improved limits of detection. The demonstrated micrometer-scale deflections of the asymmetrically nanostructured cantilevers opens up an opportunity to extend the applications of cantilever-based chemi-mechanical transduction from sensors to passive chemically controlled closed loop microfluidic MEMS powered exclusively by energy of environment-device molecular interactions (Beebe et al., 2000). In particular, asymmetrically nanostructured beams or cantilevers bearing proper receptors are foreseen as biologically controlled actuators (e.g., valves), thus constituting an essential part of an integrated analyte delivery system or a drug delivery device.

In comparison to several other coatings investigated in our study, dealloyed gold provided the most efficient transduction of chemical stimuli into mechanical responses. The implemented technology of dealloyed gold is highly compatible with conventional micro-fabrication and, we believe, can be extended to a great variety of metals and oxides. Therefore, cantilever-based transducers with nano-structured surfaces described herein will have a broad impact on the future development of biomedical sensors, actuators and “lab-on-chip” devices.

Acknowledgment

This work was supported by the U.S. Department of Energy, Environmental Management Program under grant DOE DE-FG07-98ER62718, DOE Basic Energy Sciences under grant DE-FG02-96ER14609 and by

National Science Foundation under Grant CHE-9320461. The authors gratefully acknowledge James Corbeil and Gerald DeVault for their help with AFM and SEM imaging and Dr. Thomas Green for synthesizing the HM- β -CD.

References

- M.K. Baller, H.P. Lang, J. Fritz, C. Gerber, J.K. Gimzewski, U. Drechsler, H. Rothuizen, M. Despont, P. Vettiger, F.M. Battiston, J.P. Ramseyer, P. Fornaro, E. Meyer, and H.J. Guntherodt, *Ultramicroscopy* **82**, 1–9 (2000).
- D.J. Beebe, J.S. Moore, J.M. Bauer, Q. Yu, R.H. Liu, C. Devadoss, and B.H. Jo, *Nature* **404**, 6 (2000).
- R. Berger, E. Delamarche, H.P. Lang, C. Gerber, J.K. Gimzewski, E. Meyer, and H.J. Guntherodt, *Science* **276**, 2021–2024 (1997).
- T. Betts, C. Tipple, P.G. Datskos, and M.J. Sepaniak, *Analytica Chimica Acta* **422**, 89–99 (2000).
- H.J. Butt, *Journal of Colloid & Interface Science* **180**, 251–260 (1996).
- P.G. Datskos and I. Sauer, *Sensors & Actuators B Chemical* **61**, 75–82 (1999).
- F.R. de Boer, R. Boom, W.C.M. Mattens, A.R. Miedema, and A.K. Niessen, *Cohesion in Metals* (North-Holland, Amsterdam, 1988).
- E. Evans and K. Ritchie, *Biophysical Journal* **72**, 1541–1555 (1997).
- B. Fagan, M.J. Sepaniak, and Z. Ben Xue, *Talanta* **53**, 599–608 (2000).
- L.J.D. Frink and F. van Swol, *Langmuir* **15**, 3296–3301 (1999).
- L.J.D. Frink and F. van Swol, *Colloids & Surfaces A: Physicochemical & Engineering Aspects* **162**, 25–36 (2000).
- J. Fritz, M.K. Baller, H.P. Lang, H. Rothuizen, P. Vettiger, E. Meyer, H.J. Guntherodt, C. Gerber, and J.K. Gimzewski, *Science* **288**, 316–318 (2000).
- K.C. Grabar, K.J. Allison, B.E. Baker, R.M. Bright, K.R. Brown, R.G. Freeman, A.P. Fox, C.D. Keating, M.D. Musick, and M.J. Natan, *Langmuir* **12**, 2353–2361 (1996).
- G. Guilbault, B. Hock, and R. Schmid, *Biosensors and Bioelectronics* **7**, 411 (1992).
- J.G.E. Harris, D.D. Awschalom, K.D. Maranowski, and A.C. Gossard, *Review of Scientific Instruments* **67**, 3591–3593 (1996).
- J. Israelachvili, *Intermolecular and Surface Forces* (Academic Press, San Diego, 1991).
- H.F. Ji, E. Finot, R. Dabestani, T. Thundat, G.M. Brown, and P.F. Britt, *Chemical Communications* **6**, 457–458 (2000).
- G. Lang and K.E. Heusler, *Russian Journal of Electrochemistry* **31**, 759 (1995).
- N. Lavrik and D. Leckband, *Langmuir* **16**, 1842–1851 (2000).
- N.V. Lavrik, C.A. Tipple, M.J. Sepaniak, and P.G. Datskos, *Physical Chemistry Letters* **336**, 371–376 (2000).
- D. Leckband, *Nature* **376**, 617–618 (1995).
- D. Leckband, W. Muller, F.J. Schmitt, and H. Ringsdorf, *Biophysical Journal* **69**, 1162–1169 (1995).
- D.E. Leckband, F.J. Schmitt, J.N. Israelachvili, and W. Knoll, *Biochemistry* **33**, 4611–4624 (1994).
- R. Li and K. Sieradzki, *Physical Review Letters* **68**, 1168–1171 (1992).
- M. Maute, S. Raible, F.E. Prins, D.P. Kern, H. Ulmer, U. Weimar, and W. Gopel, *Sensors & Actuators, B* **58**, 505–511 (1999).
- T. Moks, L. Abrahamsen, B. Nilsson, U. Hellman, J. Sjoquist, and M. Uhlen, *European Journal of Biochemistry* **156**, 637–643 (1986).
- A.M. Moulin, S.J. Shea, and M.E. Welland, *Ultramicroscopy* **82**, 23–31 (2000).
- A.M. Moulin, S.J. Shea, R.A. Badley, P. Doyle, and M.E. Welland, *Langmuir* **15**, 8776–8779 (1999).
- V.A. Parsegian and R. Podgornik, *Colloids and Surfaces a-Physicochemical and Engineering Aspects* **130**, 345 (1997).
- R. Raiteri, G. Nelles, H.J. Butt, W. Knoll, and P. Skladal, *Sensors & Actuators, B* **61**, 213–217 (1999).
- M.T. Rojas, R. Koniger, J.F. Stoddart, and A.E. Kaifer, *Journal of the American Chemical Society* **117**, 336–343 (1995).
- S. Sivasankar, W. Briehner, N. Lavrik, B. Gumbiner, and D. Leckband, *Proceedings of the National Academy of Sciences of the United States of America* **96**, 11820–11824 (1999).
- G.G. Stoney, *Proceedings of the Royal Society of London*, **A82**, 172–177 (1909).
- T. Thundat, G.Y. Chen, R.J. Warmack, D.P. Allison, and E.A. Wachter, *Analytical Chemistry* **67**, 519–520 (1995).
- T. Thundat, P.I. Oden, and R.J. Warmack, *Microscale Thermophysical Engineering* **1**, 185–199 (1997).
- J. Varesi, J. Lai, T. Perazzo, Z. Shi, and A. Majumdar, *Applied Physics Letters* **71**, 306–308 (1997).
- F.J. von Preissig, *Journal of Applied Physics* **66**, 4262 (1989).